Nonlinear Magneto-Optical Rotation (NMOR)

2011.06.08 ランチミーティング

担当：鳥井

気体原子のスピンコヒーレンスの応用

- 原子時計（atomic clocks）
- 磁力計（magnetometers）
- 量子メモリー（quantum memory）
- スピンスクイージング（spin-squeezing）
- 量子非破壊測定（quantum nondemolition measurments）

Spectroscopy of spontaneous spin noise as a probe of spin dynamics and magnetic resonance

S. A. Crooker[1], D. G. Rickel[1], A. V. Balatsky[2] & D. L. Smith[2]

[1]*National High Magnetic Field Laboratory,* [2]*Theory Division, Los Alamos National Laboratory, Los Alamos, New Mexico 87545, USA*

Not all noise in experimental measurements is unwelcome. Certain fundamental noise sources contain valuable information about the system itself—a notable example being the inherent voltage fluctuations (Johnson noise) that exist across any resistor, which allow the temperature to be determined[1,2]. In magnetic systems, fundamental noise can exist in the form of random spin fluctuations[3,4]. For example, statistical fluctuations of N paramagnetic spins should generate measurable noise of order $\sqrt{N}$ spins, even in zero magnetic field[5,6]. Here we exploit this effect to perform perturbation-free magnetic resonance. We use off-resonant Faraday rotation to passively[7,8] detect the magnetization noise in an equilibrium ensemble of paramagnetic alkali atoms; the random fluctuations generate spontaneous spin coherences that precess and decay with the same characteristic energy and timescales as the macroscopic magnetization of an intentionally polarized or driven ensemble. Correlation spectra of the measured spin noise reveal g-factors, nuclear spin, isotope abundance ratios, hyperfine splittings, nuclear moments and spin coherence lifetimes—without having to excite, optically pump or otherwise drive the system away from thermal equilibrium. These noise signatures scale inversely with interaction volume, suggesting a possible route towards non-perturbative, sourceless magnetic resonance of small systems.

The fluctuation–dissipation theorem states that the response of a system to an external perturbation (that is, the susceptibility) can be

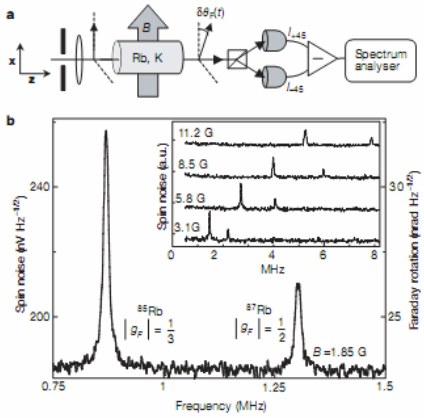

Figure 1 Spontaneous spin noise in Rb or K vapour, probed via Faraday rotation. **a**, Experimental schematic. Ground-state stochastic spin fluctuations $\delta M_z(t)$ impart polarization fluctuations $\delta\theta_F(t)$ on the detuned probe laser. **b**, Measured spectrum of spin Faraday rotation) noise from Rb vapour at temperature $T = 369$ K and magnetic field $B = 1.85$ G, showing spontaneous spin coherence peaks from ^{85}Rb and ^{87}Rb. The data are given in units of root-mean-square (r.m.s.) spectral density of voltage fluctuations (nV Hz$^{-1/2}$) measured in the photodiode bridge, and also by the r.m.s. spectral density of Faraday rotation fluctuations (nrad Hz$^{-1/2}$). The noise floor is determined primarily by photon shot noise. The laser is detuned $\Delta_{D1} = 25$ GHz from the D1 transition ($5^2S_{1/2}$ to $5^2P_{1/2}$, ~794.8 nm), ensuring negligible absorption. Inset: the ^{85}Rb and ^{87}Rb spin noise peaks measured at $\Delta_{D2} = 20$ GHz from the D2 transition ($5^2S_{1/2}$ to $5^2P_{3/2}$, ~780 nm). The magnetic field B is incremented in steps of 2.7 G, and $T = 369$ K. Plots offset vertically for clarity. a.u., arbitrary units.

High Bandwidth Atomic Magnetometery with Continuous Quantum Nondemolition Measurements

V. Shah, G. Vasilakis, and M. V. Romalis

Department of Physics, Princeton University, Princeton, New Jersey 08544, USA

(Received 14 July 2009; published 5 January 2010)

We describe an experimental study of spin-projection noise in a high sensitivity alkali-metal magnetometer. We demonstrate a fourfold improvement in the measurement bandwidth of the magnetometer using continuous quantum nondemolition measurements. Operating in the scalar mode with a measurement volume of 2 cm^3 we achieve magnetic field sensitivity of 22 fT/Hz$^{1/2}$ and a bandwidth of 1.9 kHz with a spin polarization of only 1%. Our experimental arrangement is naturally backaction evading and can be used to realize sub-fT sensitivity with a highly polarized spin-squeezed atomic vapor.

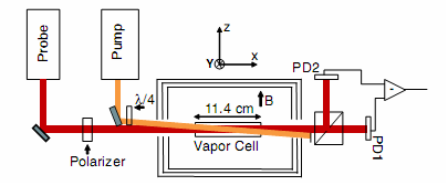

FIG. 1 (color online). Apparatus for high-bandwidth QND scalar magnetometry.

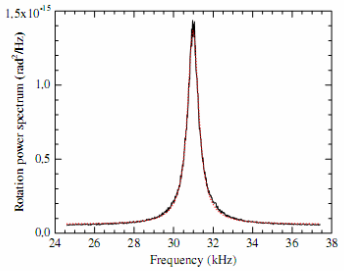

FIG. 2 (color online). Measured spin noise power spectrum of unpolarized atoms (solid line) with a fit to a Lorentzian plus flat photon shot noise background (dashed line). The averaging time for the noise spectrum is 350 s.

Polarized Alkali-Metal Vapor with Minute-Long Transverse Spin-Relaxation Time

M. V. Balabas,[1] T. Karaulanov,[2] M. P. Ledbetter,[2,*] and D. Budker[2,3]

[1]*S. I. Vavilov State Optical Institute, St. Petersburg, 199034 Russia*

[2]*Department of Physics, University of California at Berkeley, Berkeley, California 94720-7300, USA*

[3]*Nuclear Science Division, Lawrence Berkeley National Laboratory, Berkeley California 94720, USA*

(Received 7 May 2010; published 12 August 2010)

We demonstrate lifetimes of Zeeman populations and coherences in excess of 60 sec in alkali-metal vapor cells with inner walls coated with an alkene material. This represents 2 orders of magnitude improvement over the best paraffin coatings. We explore the temperature dependence of cells coated with this material and investigate spin-exchange relaxation-free magnetometry in a room-temperature environment, a regime previously inaccessible with conventional coating materials.

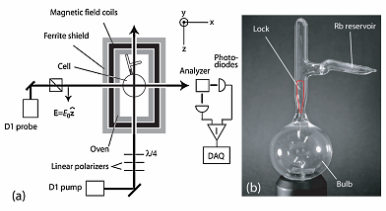

FIG. 1 (color online). Experimental setup: (a) Four mu-metal shields (not shown) surround the ferrite shield. The ferrite shield is a cylinder, 15.2 cm long and 11.4 cm in diameter (inner dimensions) with 1.3 cm thick walls. A set of coils provides control over the magnetic fields. The oven was temperature controlled by running ac current through twisted-pair copper wire. (b) Photo of the coated cell.

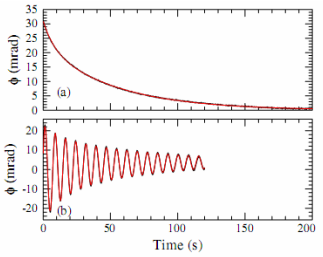

FIG. 2 (color online). (a) Decay of longitudinal polarization. The red trace overlaying the data is a fit to two decaying exponentials, with fast and slow decay times of 8 and 53 seconds, respectively. (b) Response of alkali-metal spin polarization to a transient of the magnetic field. The fast and slow decay times are 13 and 77 sec.

REVIEWS OF MODERN PHYSICS, VOLUME 74, OCTOBER 2002

Resonant nonlinear magneto-optical effects in atoms*

D. Budker†

Department of Physics, University of California, Berkeley, California 94720-7300 and Nuclear Science Division, Lawrence Berkeley National Laboratory, Berkeley, California 94720

W. Gawlik‡

Instytut Fizyki im. M. Smoluchowskiego, Uniwersytet Jagielloński, Reymonta 4, 30-059 Kraków, Poland

D. F. Kimball,§ S. M. Rochester,‖ and V. V. Yashchuk¶

Department of Physics, University of California, Berkeley, California 94720-7300

A. Weis**

Département de Physique, Université de Fribourg, Chemin du Musée 3, CH-1700 Fribourg, Switzerland

(Published 20 November 2002)

The authors review the history, current status, physical mechanisms, experimental methods, and applications of nonlinear magneto-optical effects in atomic vapors. They begin by describing the pioneering work of Macaluso and Corbino over a century ago on linear magneto-optical effects (in which the properties of the medium do not depend on the light power) in the vicinity of atomic resonances. These effects are then contrasted with various nonlinear magneto-optical phenomena that have been studied both theoretically and experimentally since the late 1960s. In recent years, the field of nonlinear magneto-optics has experienced a revival of interest that has led to a number of developments, including the observation of ultranarrow (1-Hz) magneto-optical resonances, applications in sensitive magnetometry, nonlinear magneto-optical tomography, and the possibility of a search for parity- and time-reversal-invariance violation in atoms.

Atomic Physics
(Budker, Kimball & DeMille)

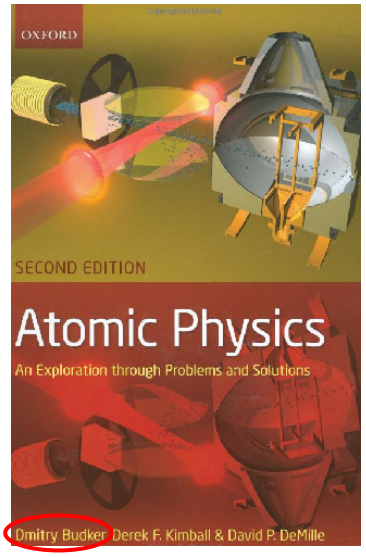

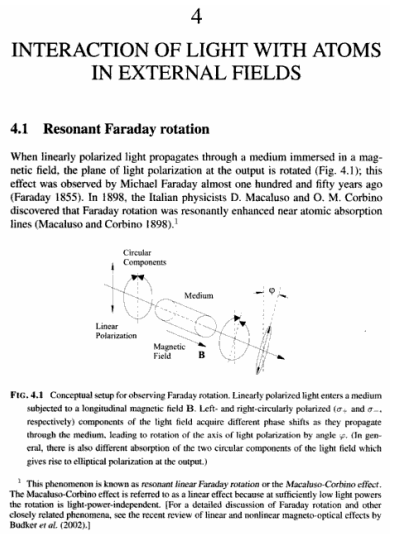

4

INTERACTION OF LIGHT WITH ATOMS IN EXTERNAL FIELDS

4.1 Resonant Faraday rotation

When linearly polarized light propagates through a medium immersed in a magnetic field, the plane of light polarization at the output is rotated (Fig. 4.1); this effect was observed by Michael Faraday almost one hundred and fifty years ago (Faraday 1855). In 1898, the Italian physicists D. Macaluso and O. M. Corbino discovered that Faraday rotation was resonantly enhanced near atomic absorption lines (Macaluso and Corbino 1898).[1]

FIG. 4.1 Conceptual setup for observing Faraday rotation. Linearly polarized light enters a medium subjected to a longitudinal magnetic field **B**. Left- and right-circularly polarized (σ_+ and σ_-, respectively) components of the light field acquire different phase shifts as they propagate through the medium, leading to rotation of the axis of light polarization by angle φ. (In general, there is also different absorption of the two circular components of the light field which gives rise to elliptical polarization at the output.)

[1] This phenomenon is known as *resonant linear Faraday rotation* or the *Macaluso-Corbino effect*. The Macaluso-Corbino effect is referred to as a linear effect because at sufficiently low light powers the rotation is light-power-independent. [For a detailed discussion of Faraday rotation and other closely related phenomena, see the recent review of linear and nonlinear magneto-optical effects by Budker *et al.* (2002).]

電場と分極の線形関係

$$\boldsymbol{P} = \varepsilon_0 \chi(\omega) \boldsymbol{E}$$

$\chi(\omega) = \chi'(\omega) + i\chi''(\omega)$ ：複素電気感受率

$$\boldsymbol{D} \equiv \boldsymbol{P} + \varepsilon_0 \boldsymbol{E} = \varepsilon_0 (1+\chi)\boldsymbol{E} = \varepsilon \boldsymbol{E}$$

電場の波動方程式は

$$\nabla^2 \boldsymbol{E} = \varepsilon\mu_0 \frac{\partial^2 \boldsymbol{E}}{\partial t^2} = \varepsilon_0\mu_0(1+\chi)\frac{\partial^2 \boldsymbol{E}}{\partial t^2} = \frac{1+\chi}{c^2}\frac{\partial^2 \boldsymbol{E}}{\partial t^2}$$

分散性媒質中の電磁波

媒質中をz軸方向に伝播する電磁波（電場）を

$$\boldsymbol{E}(z,t) = \hat{\varepsilon}E(z,t) = \hat{\varepsilon}E_0 \exp\left[i(kz - \omega t)\right]$$ $\hat{\varepsilon}$：偏光ベクトル

と表すことにすると、電場の波動方程式より

$$k^2 = \frac{\omega^2}{c^2}(1+\chi(\omega)) = k_0^2(1+\chi(\omega)) \quad \left(k_0 \equiv \frac{\omega}{c}\right)$$

真空中の波数

$|\chi(\omega)| << 1$ と仮定すると、

$$k = k_0\sqrt{1+\chi(\omega)} \cong k_0\left(1 + \frac{\chi'(\omega)}{2} + i\frac{\chi''(\omega)}{2}\right)$$

吸収係数と屈折率

kの値を代入すると、電場は

$$\boldsymbol{E}(\boldsymbol{r},t) = \hat{\varepsilon}E_0 \exp\left(-\frac{\alpha}{2}z\right)\exp\left[i\left(k'z - \omega t\right)\right]$$

$\alpha = k_0\chi''$：吸収係数　　$k' = nk_0$　　$n = 1 + \frac{\chi'}{2}$：屈折率

強度の位置依存性は　　光学密度（Optical Density）

$$I(l) = I_0 \exp(-\alpha l) = I_0 \exp\left(-l/l_0\right)$$

$l_0 = 1/\alpha$：吸収長（absorption length）　強度が1/eになる長さ

分極のミクロな古典モデル
（調和振動子）

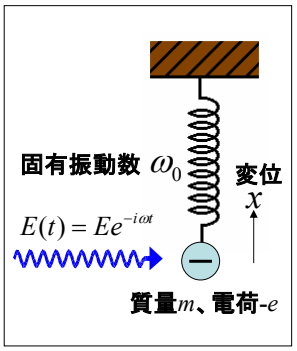

$$m\frac{d^2x}{dt^2}+2m\gamma\frac{dx}{dt}+m\omega_0^2x=-eEe^{-i\omega t}$$

$x=x(\omega)e^{-i\omega t}$ とおいて代入すると

$$x(\omega)=\frac{eE}{m}\cdot\frac{1}{\omega^2+2i\gamma\omega-\omega_0^2}$$

マクロな分極は

$$Pe^{-i\omega t}=-Nex=\varepsilon_0\left[-\frac{Ne^2}{\varepsilon_0 m}\cdot\frac{1}{\omega^2+2i\gamma\omega-\omega_0^2}\right]Ee^{-i\omega t}$$

N：原子数密度

$\left[\cdots\right]=\chi(\omega)$

$$\chi(\omega)=-\frac{Ne^2}{\varepsilon_0 m}\cdot\frac{1}{\omega^2+2i\gamma\omega-\omega_0^2}$$

$\omega\approx\omega_0$（共鳴付近）のときは

$$\chi(\omega)=-\frac{Ne^2}{2m\varepsilon_0\omega_0}\cdot\frac{1}{\omega-\omega_0+i\gamma}\propto-\frac{1}{\Delta+i\gamma}$$

$$(\Delta\equiv\omega-\omega_0)$$

$$\begin{cases}\chi'(\omega)=-\chi''_{\max}\dfrac{\Delta\gamma}{\Delta^2+\gamma^2}\\ \chi''(\omega)=\chi''_{\max}\dfrac{\gamma^2}{\Delta^2+\gamma^2}\end{cases}$$

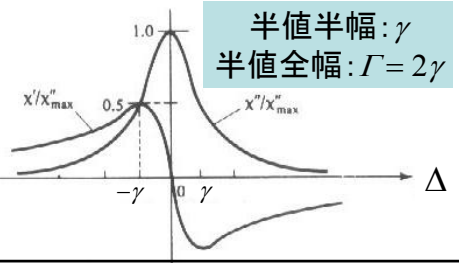

半値半幅：γ
半値全幅：$\Gamma=2\gamma$

円偏光の複屈折（birefringence）と二色性（dichroism）

$$\boldsymbol{E}_{\sigma+}(t) = -\frac{E_0}{\sqrt{2}}\left(\hat{\boldsymbol{\varepsilon}}_x \cos\omega t + \hat{\boldsymbol{\varepsilon}}_y \sin\omega t\right) \xrightarrow{\text{複素表示}} -\frac{E_0}{\sqrt{2}}\left(\hat{\boldsymbol{\varepsilon}}_x + i\hat{\boldsymbol{\varepsilon}}_y\right)e^{-i\omega t} = \hat{\boldsymbol{\varepsilon}}_+ E_0 e^{-i\omega t}$$

$$\boldsymbol{E}_{\sigma-}(t) = +\frac{E_0}{\sqrt{2}}\left(\hat{\boldsymbol{\varepsilon}}_x \cos\omega t - \hat{\boldsymbol{\varepsilon}}_y \sin\omega t\right) \xrightarrow{\text{複素表示}} +\frac{E_0}{\sqrt{2}}\left(\hat{\boldsymbol{\varepsilon}}_x - i\hat{\boldsymbol{\varepsilon}}_y\right)e^{-i\omega t} = \hat{\boldsymbol{\varepsilon}}_- E_0 e^{-i\omega t}$$

$$\hat{\varepsilon}_+ = -\frac{1}{\sqrt{2}}\left(\hat{\varepsilon}_x + i\hat{\varepsilon}_y\right) \qquad \hat{\varepsilon}_- = \frac{1}{\sqrt{2}}\left(\hat{\varepsilon}_x - i\hat{\varepsilon}_y\right)$$

$$\Longleftrightarrow$$

$$\hat{\varepsilon}_x = -\frac{1}{\sqrt{2}}\left(\hat{\varepsilon}_+ - \hat{\varepsilon}_-\right) \qquad \hat{\varepsilon}_y = \frac{i}{\sqrt{2}}\left(\hat{\varepsilon}_+ + \hat{\varepsilon}_-\right)$$

円偏光の伝搬

$$\boldsymbol{E}_{\sigma\pm}(z,t) = \hat{\boldsymbol{\varepsilon}}_\pm E_0 \exp\left(-\frac{\alpha_\pm}{2}z\right)\exp\left[i\left(k'_\pm z - \omega t\right)\right] \quad (\alpha_\pm = k_0\chi''_\pm,\ k'_\pm = n_\pm k_0)$$

$\Delta n \equiv n_+ - n_- \neq 0$ なら複屈折性あり。　$\Delta\alpha \equiv \alpha_+ - \alpha_+ \neq 0$ なら二色性あり。

The Faraday and Voigt effect

入射光はx方向に直線偏光しているとする。

$$\hat{\varepsilon}_x = -\frac{1}{\sqrt{2}}\left(\hat{\varepsilon}_+ - \hat{\varepsilon}_-\right)$$

σ+とσ-の半々の重ね合わせ

長さlの媒質を通過後の出力光は

$$\boldsymbol{E}(l,t) = -\frac{1}{\sqrt{2}}\left(\boldsymbol{E}_{\sigma+}(l,t) - \boldsymbol{E}_{\sigma-}(l,t)\right)$$

位相90度遅れ

$$= \left[\bar{E}(\hat{\boldsymbol{\varepsilon}}_x\cos\varphi - \hat{\boldsymbol{\varepsilon}}_y\sin\varphi) + i\Delta E(\hat{\boldsymbol{\varepsilon}}_x\sin\varphi + \hat{\boldsymbol{\varepsilon}}_y\cos\varphi)\right] \times e^{i\left(\frac{n_+ + n_-}{2}k_0 l - \omega t\right)}$$

直交

$$\varphi = \frac{\Delta n}{2}k_0 l = \pi\frac{(n_+ - n_-)l}{\lambda}$$

$$\bar{E} \equiv (e^{-\frac{\alpha_+ l}{2}} + e^{-\frac{\alpha_- l}{2}})E_0/2,\ \Delta E \equiv (e^{-\frac{\alpha_+ l}{2}} - e^{-\frac{\alpha_- l}{2}})E_0/2$$

$\Delta\alpha \neq 0\,(\Delta E \neq 0)$（二色性あり）ならば楕円偏光

$\Delta\alpha = 0\,(\Delta E = 0)$（二色性なし）ならば直線偏光

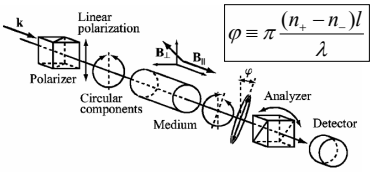

$$\varphi \equiv \pi\frac{(n_+ - n_-)l}{\lambda}$$

FIG. 1. The Faraday and Voigt effects. In the Faraday effect, light, after passing through a linear polarizer, enters a medium subjected to a longitudinal magnetic field $\mathbf{B}_\parallel$ ($\mathbf{B}_\perp$=0). Left- and right-circularly polarized components of the light (equal in amplitude for linearly polarized light) acquire different phase shifts, leading to optical rotation. A difference in absorption between the two components induces ellipticity in the output light. The intensity of the transmitted light with a particular polarization is detected depending on the orientation of the analyzer relative to the polarizer. Analyzer orientation varies with the type of experiment being performed. In forward-scattering experiments (Sec. II.B), the analyzer is crossed with the input polarizer, so that only light of the orthogonal polarization is detected. In the "balanced polarimeter" arrangement (Sec. XI.B), a polarizing beam splitter oriented at $\pi/4$ to the input polarizer is used as an analyzer. In this case, the normalized differential signal between the two channels of the analyzer depends on the rotation of light polarization while being insensitive to induced ellipticity. The Voigt effect is similar except that instead of a longitudinal magnetic field, a transverse field $\mathbf{B}_\perp$ ($\mathbf{B}_\parallel$=0) is applied. Here optical rotation and induced ellipticity are due to differential absorption and phase shifts of orthogonal linearly polarized components of the input light (Sec. VI).

Rev. Mod. Phys. **70**, 1153 (2002)

The Macaluso Corbino effect

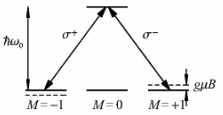

FIG. 2. An $F=1\rightarrow F'=0$ atomic transition. In the presence of a longitudinal magnetic field, the Zeeman sublevels of the ground state are shifted in energy by $g\mu BM$. This leads to a difference in resonance frequencies for left- (σ^+) and right- (σ^-) circularly polarized light.

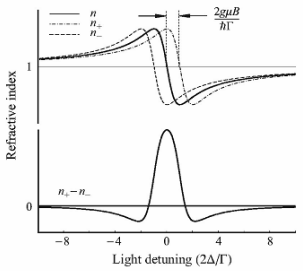

FIG. 3. The dependence of the refractive index on light frequency detuning Δ in the absence (n) and in the presence ($n_\pm$) of a magnetic field. Shown is the case of $2g\mu B=\hbar\Gamma$ and a Lorentzian model for line broadening. The lower curve shows the difference of refractive indices for the two circular polarization components. The spectral dependence of this difference gives the characteristic spectral shape of the linear magneto-optical rotation (the Macaluso-Corbino effect).

$$\varphi=\pi\frac{(n_+-n_-)l}{\lambda}=\frac{k_0(n_+-n_-)l}{2}$$

$$n_\pm=1+\frac{\chi'_\pm}{2}=1-\frac{1}{2}\chi''_{\max}\frac{\Delta_\pm\gamma}{\Delta_\pm^2+\gamma^2}$$

$$\Delta_\pm=\omega-(\omega_0\pm\frac{g\mu B}{\hbar})=\Delta\mp\frac{g\mu B}{\hbar}$$

$$\varphi=\frac{k_0\chi''_{\max}l}{4}\left[\frac{\left(\Delta+\frac{g\mu B}{\hbar}\right)\gamma}{\left(\Delta+\frac{g\mu B}{\hbar}\right)^2+\gamma^2}-\frac{\left(\Delta-\frac{g\mu B}{\hbar}\right)\gamma}{\left(\Delta-\frac{g\mu B}{\hbar}\right)^2+\gamma^2}\right]\xrightarrow{\Delta=0}\frac{1}{2}\frac{b}{1+b^2}\frac{l}{l_0}\left(b\equiv\frac{g\mu B}{\hbar\gamma}\right)$$

NMOR signal for 85Rb (F=3 to F')

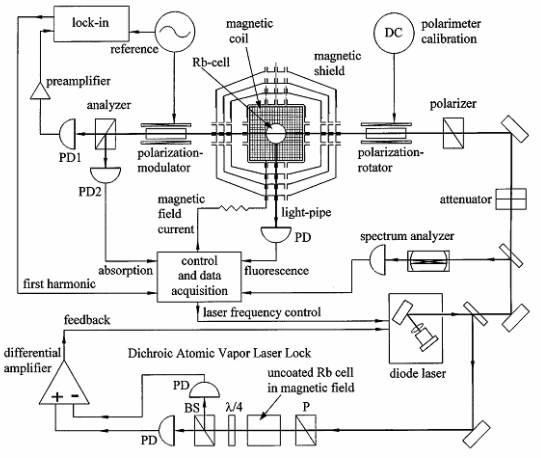

FIG. 1. Schematic diagram of the experimental arrangement.

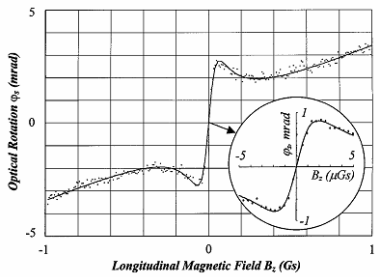

FIG. 3. Optical rotation dependence on the longitudinal magnetic field. Light intensity: ≈100 μW/cm^2; the laser is tuned to the peak of the $F=3$ component of NMOE, corresponding to a ≈150 MHz high frequency detuning from the peak of the fluorescence (Fig. 2). The solid line is a fit to the model described in the text. The inset shows a detailed scan of the near-zero B_z-field region.

D. Budker, et. al, Phys. Rev. Lett. **81**, 5788 (1998)

Nonlinear Magneto-Optical Effect
A. Bennett-structure effect

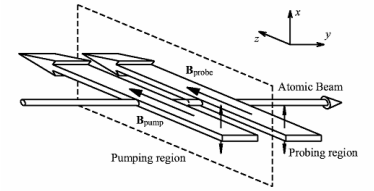

FIG. 11. Conceptual two-region experimental arrangement with separated optical pumping and probing regions used to treat Bennett-structure effects in nonlinear magneto-optical rotation. Pump and probe light beams are initially linearly polarized along x, the atomic beam propagates in the $\hat{y}$ direction, and the magnetic fields are oriented along the direction of light propagation ($\hat{z}$).

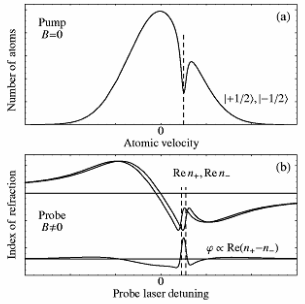

FIG. 12. The Bennett-structure effect on a 1/2→1/2 transition in which the upper state decays to levels other than the lower state; $\mathbf{B}_{\text{pump}}=0$, $\mathbf{B}_{\text{probe}}\neq 0$. (a) In the pump region, monochromatic laser light produces Bennett holes in the velocity distributions of atoms in the lower state $|+1/2\rangle$, $|-1/2\rangle$ sublevels. Since there is no magnetic field, the holes occur in the same velocity group (indicated by the dashed line) for each sublevel. (b) In the probe region, a magnetic field is applied, shifting n_+ and n_- relative to each other (upper trace). The real part of the indices of refraction are shown so that the features in plot (a) correspond to dispersive shapes in this plot. The shifted central detunings of the Bennett-structure features are indicated by the dashed lines. Polarization rotation of the probe laser light is proportional to the difference $\mathrm{Re}(n_+ - n_-)$ (lower trace). Features due to the Doppler distribution and the Bennett holes can be seen. Since the Bennett related feature is caused by the removal of atoms from the Doppler distribution, the sign of rotation due to this effect is opposite to that of the linear rotation. From Budker, Kimball, *et al.*, 2002a.

プローブ光自身がポンプ光として働く
→速度分布に自然幅程度（1-10MHz）のディップ
→磁場を掃引すると、自然幅程度の分散型信号が観測される

Alignment of atoms due to optical pumping (linear polarization)

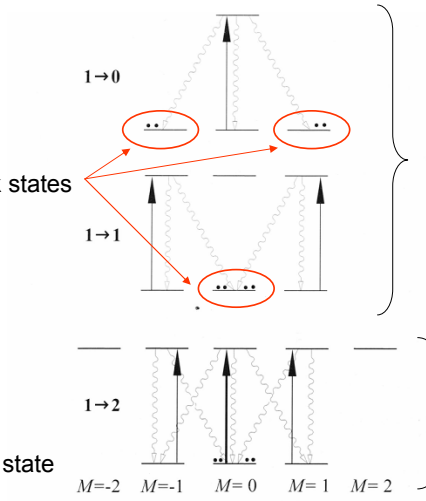

FIG. 3.14 Illustration of the effects of optical pumping with linearly polarized (π) light on the populations of ground state Zeeman sublevels for closed $J = 1 \rightarrow J' = 0, 1, 2$ transitions.

量子化軸を変えて見ると…

量子化軸が光の偏光方向

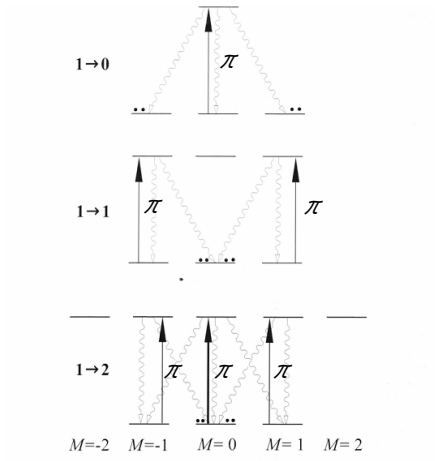

FIG. 3.14 Illustration of the effects of optical pumping with linearly polarized (π) light on the populations of ground state Zeeman sublevels for closed $J = 1 \rightarrow J' = 0, 1, 2$ transitions.

量子化軸が光の進行方向

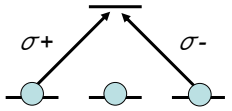

Dark state: $|0>, \frac{1}{\sqrt{2}}(|-1>-|+1>)$

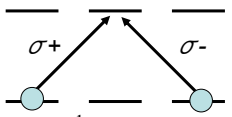

Dark state: $\frac{1}{\sqrt{2}}(|-1>-|+1>)$

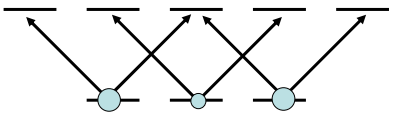

Nonlinear Magneto-Optical Effect
B. Coherence effect (dark resonance)

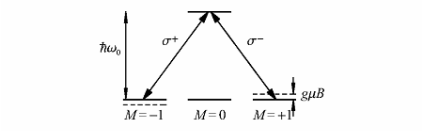

FIG. 2. An $F=1 \rightarrow F'=0$ atomic transition. In the presence of a longitudinal magnetic field, the Zeeman sublevels of the ground state are shifted in energy by $g\mu BM$. This leads to a difference in resonance frequencies for left- (σ^+) and right- (σ^-) circularly polarized light.

プローブ光を吸収により、原子はdark state に光ポンピングされる

$$|\Psi>_{\text{Dark}} = \frac{1}{\sqrt{2}}(|-1>-|+1>)$$

→プローブ光の透明化（Dark resonance）

しかし、磁場が存在すると、dark stateが回転する（ラーモアの歳差運動）

$$|\Psi>_{\text{Dark}} = \frac{1}{\sqrt{2}}\left(e^{+i\frac{g\mu B}{\hbar}t}|-1>-|e^{-i\frac{g\mu B}{\hbar}t}|+1>\right)$$

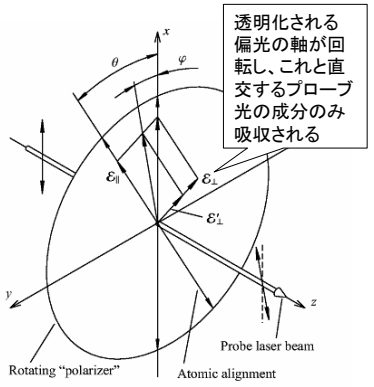

FIG. 13. An optically thin sample of aligned atoms precessing in a magnetic field, which can be thought of as a thin rotating polaroid film that is transparent to light polarized along its axis ($\mathcal{E}_\parallel$) and slightly absorbent for the orthogonal polarization ($\mathcal{E}_\perp$). Here $\mathcal{E}_\parallel$ and $\mathcal{E}_\perp$ are the light electric-field components. The effect of such a "polarizer" is to rotate light polarization by an angle $\varphi \propto \sin 2\theta$). The figure is drawn assuming that a magnetic field is directed along $\hat{\mathbf{z}}$. Adapted from Budker, Orlando, and Yashchuk (1999).

RbセルのNMOR信号（@0.1G）

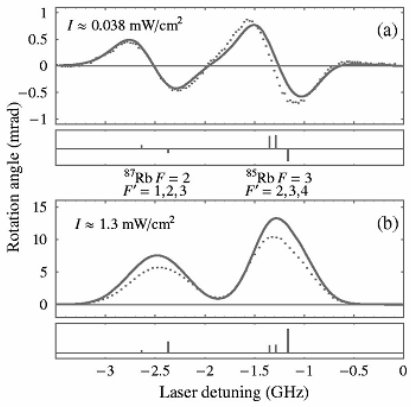

FIG. 15. Comparison of experimental NMOR spectra obtained by Budker *et al.* (2000a) to density-matrix calculations performed in the same work for a natural mixture of Rb isotopes contained in an uncoated buffer-gas-free vapor cell. Solid curves, theory (without free parameters). Offset vertical bars indicate the central frequencies and calculated relative contributions of different hyperfine components ($F \rightarrow F'$) to the overall rotation. Laser detuning is relative to the $D2$ line center. Magnetic field is ~0.1 G (at which NMOR is relatively large and coherence effects dominate), laser beam diameter is ~3.5 mm, and Rb density is ~10^{10} cm^{-3}. Residual discrepancies between data and theory may be due to nonuniform spatial distribution of light intensity. Note that at low light power (a), the sign of rotation for $F \rightarrow F+1$ transitions is opposite to that for $F \rightarrow F-1, F$ transitions, whereas at high light power (b) the sign of rotation is the same for all hyperfine transitions. From Budker, Kimball, *et al.*, 2000a.

プローブ光強度が弱いとき、NMOR信号はcoherent effectでよく説明できる（図（a））。しかし、プローブ光強度が強くなると、偏光の回転は大きくなり、極性は遷移に依存しなくなる（図（b））。何か別のメカニズムが働いているはずである。

Nonlinear Magneto-Optical Effect
C. Alignment to orientation conversion

①光ポンピング（Alignmnet）

$$|\Psi(0)\rangle = |\Psi\rangle_{\text{Dark}} = \frac{1}{\sqrt{2}}\left(|-1\rangle - |+1\rangle\right)$$

②磁場による歳差運動（Lamor precession）

$$|\Psi(t)\rangle = \frac{1}{\sqrt{2}}\left(|-1\rangle - e^{-i\frac{2g\mu B}{\hbar}t}|+1\rangle\right)$$

$$\approx |\Psi\rangle_{\text{Dark}} - i\Omega_L t\,|\Psi\rangle_{\text{Bright}} \quad (\Omega_L t << 1)$$

$$\Omega_L \equiv \frac{2g\mu B}{\hbar}$$ ラーモア周波数 $$|\Psi\rangle_{\text{Bright}} = \frac{1}{\sqrt{2}}\left(|-1\rangle + |+1\rangle\right)$$

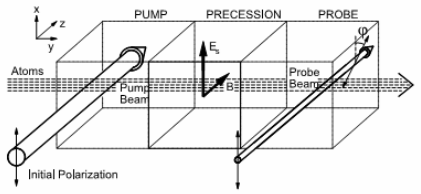

FIG. 3. Schematic diagram of an experiment with separated pump, precession, and probe regions. Atoms move with constant velocity in the $\hat{y}$ direction.

D. Budker, et. al, Phys. Rev. Lett. **85**, 2088 (2000)

③Bright stateの光シフト（light shift）によるorientation

$$|\Psi(t)\rangle \approx |\Psi\rangle_{\text{Dark}} + (-i\Omega_L t)\,e^{-i\frac{\Delta E_L}{\hbar}t}\,|\Psi\rangle_{\text{Bright}} \approx |\Psi\rangle_{\text{Dark}} - \alpha\,|\Psi\rangle_{\text{Bright}}$$

phase shift due to light shift　　実数

light shift $\left(\Delta E_L = \frac{\Omega_p^2}{2\Delta}\right)$

$$= \frac{1}{\sqrt{2}}\left[(1-\alpha)\,|-1\rangle - (1+\alpha)\,|+1\rangle\right]$$

M=-1とM=+1の分布数に偏り（orientation）
→circular birefringence

3振子の連成振動

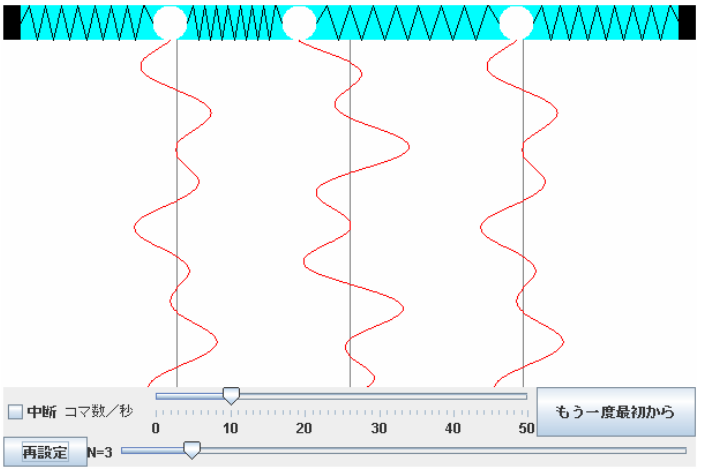

http://www.phys.u-ryukyu.ac.jp/~maeno/wave/renseiN.html

3つの固有モード

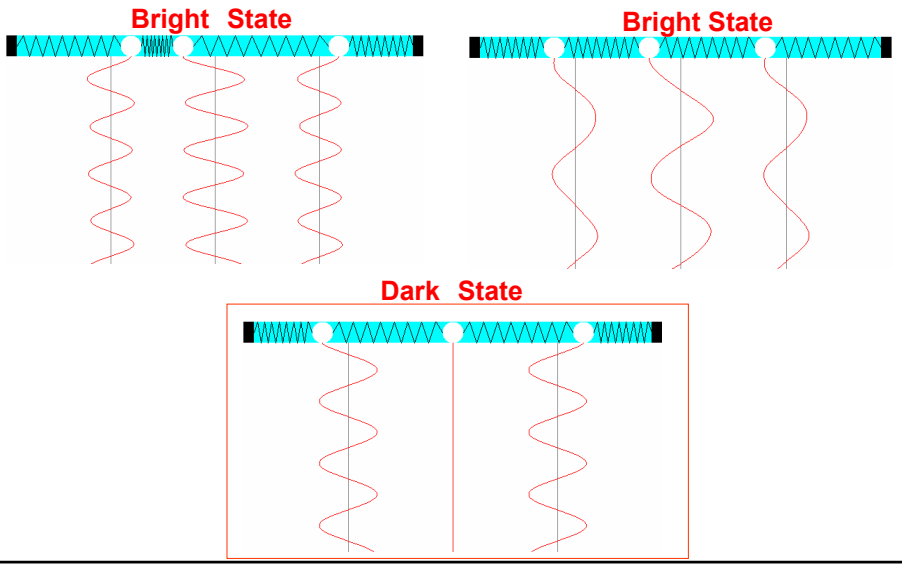

3準位原子とレーザー光との相互作用

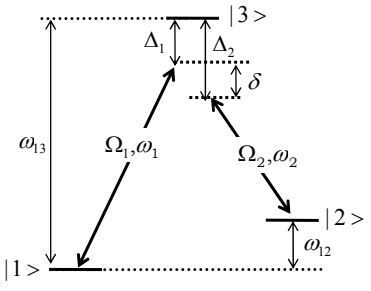

$$\hat{H} = -\delta\,|2><2| - \Delta_1\,|3><3| + \frac{\Omega_1}{2}[|1><3| + |3><1|] + \frac{\Omega_2}{2}[|2><3| + |3><2|]$$

$$|\psi> = c_1(t)\,|1> + c_2(t)\,|2> + c_3(t)\,|3>$$

$$i\hbar\frac{d}{dt}\begin{pmatrix} c_1 \\ c_2 \\ c_3 \end{pmatrix} = \frac{\hbar}{2}\begin{pmatrix} 0 & 0 & \Omega_1 \\ 0 & -2\delta & \Omega_2 \\ \Omega_1 & \Omega_2 & -2\Delta_1 \end{pmatrix}\begin{pmatrix} c_1 \\ c_2 \\ c_3 \end{pmatrix}$$

固有方程式 $$\det\begin{vmatrix} -\lambda & 0 & \Omega_1 \\ 0 & -2\delta-\lambda & \Omega_2 \\ \Omega_1 & \Omega_2 & -2\Delta_1-\lambda \end{vmatrix} = 0 \rightarrow \lambda = 0, -\Delta_1 \pm \sqrt{\Delta_1^2 + \Omega_1^2 + \Omega_2^2}$$

$$|\psi>_{\mathrm{Dark}} = \frac{1}{\sqrt{\Omega_1^2 + \Omega_2^2}}(\Omega_2\,|1> - \Omega_2\,|2>)$$

3準位原子とレーザー光との相互作用

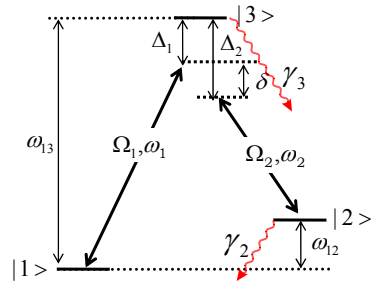

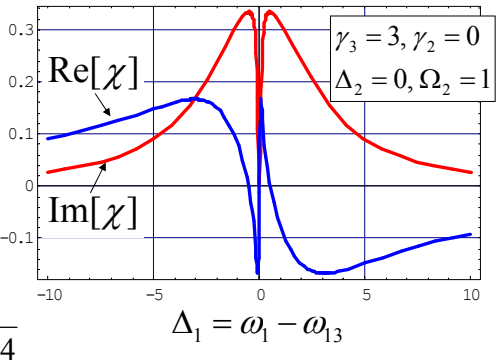

$$\Gamma_{12} = \gamma_2 - i\delta$$
$$\Gamma_{13} = \gamma_3 - i\Delta_1$$
$$\chi \propto \frac{i\Gamma_{12}}{\Gamma_{12}\Gamma_{13} + \Omega_2^2/4}$$

Applications of three-level systems

- **EIT（Electromagnetically Induced Transparency）**
- **STIRAP (Stimulated Raman Adiabatic Passage)**
- **storage of light / single photon generator**
- **ultraslow light propagation**

Wigner-Eckart
（ウィグナー・エッカルト）の定理

【JJサクライの表記法】

$$<\alpha', j', m' \mid T_q^{(k)} \mid \alpha, j, m> = <jk; mq \mid jk; j'm'> \frac{<\alpha' j' \| T_q^{(k)} \| \alpha j>}{\sqrt{2j+1}}$$

【超微細構造がある原子の電気双極子遷移に適用した場合】

原子の励起状態　　原子の基底状態

$$<F_e, M_e \mid T_q^{(1)} \mid F_g, M_g> = <F_g 1; M_g\ q \mid F_g 1; F_e M_e> \frac{<F_e \| T_q^{(1)} \| F_g>}{\sqrt{2F_g+1}}$$

電気双極子相互作用（一階の既約テンソル演算子）

$$T_q^{(1)} \equiv \begin{cases} z & (q=0:\ \pi\ \text{偏光}) \\ -(x+iy)/\sqrt{2} & (q=+1:\sigma^+\text{偏光}) \\ (x-iy)/\sqrt{2} & (q=-1:\sigma^-\text{偏光}) \end{cases}$$

$$|F_g 1; M_g q> \equiv |F_g, M_g> \otimes |1, q>$$

原子の基底状態　　光子の状態（k=1、q=-1,0,+1）

$|F_g 1; F_e M_e>$　基底状態の原子の角運動量と光子の角運動量を合成した状態（励起状態に対応）

|Fg,Mg>と|1,q>からどのように |Fe,Me>が構成されるか?

<F_g= 2の場合>

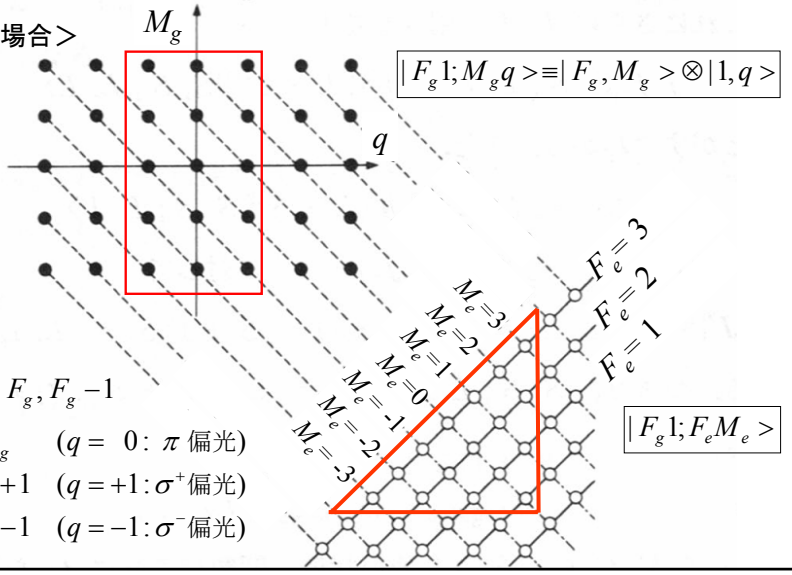

$$F_e = F_g + 1, F_g, F_g - 1$$

$$M_e = \begin{cases} M_g & (q=0:\ \pi\ \text{偏光}) \\ M_g + 1 & (q=+1:\sigma^+\text{偏光}) \\ M_g - 1 & (q=-1:\sigma^-\text{偏光}) \end{cases}$$

I=3/2(Li7,Na23,K39,Rb87)

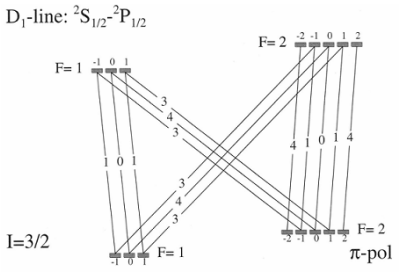

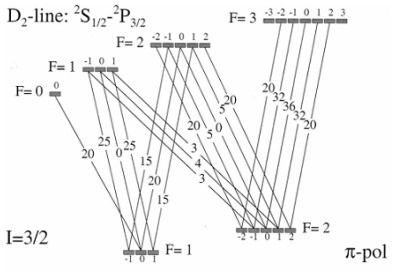

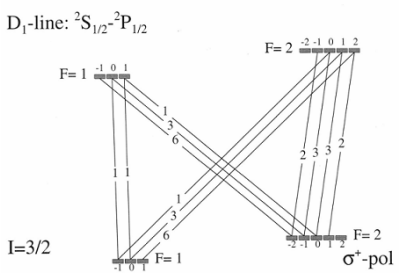

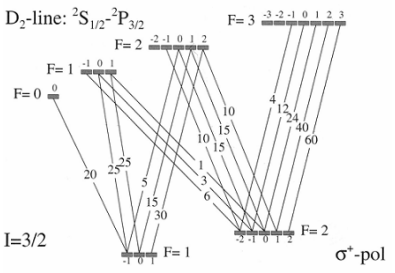

I=5/2(Rb85)

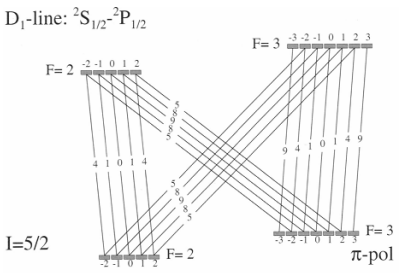

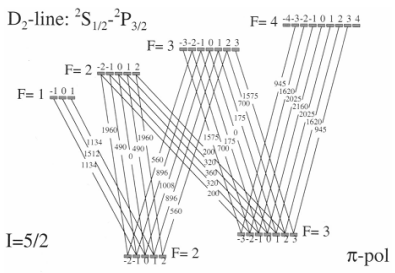

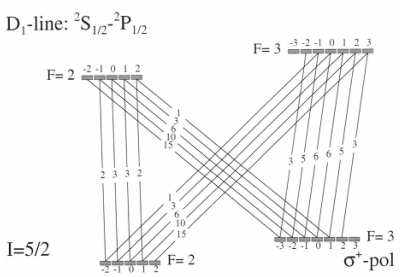

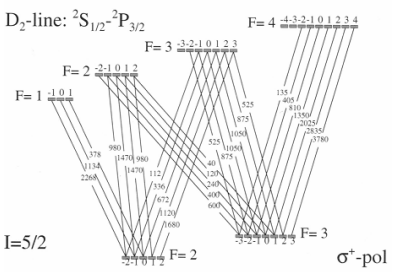

Electron EDM: A test for theories beyond the Standard Model

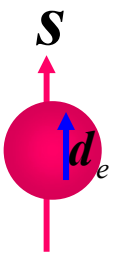

e-EDM: electron eternal dipole moment (aliened to the electron spin)

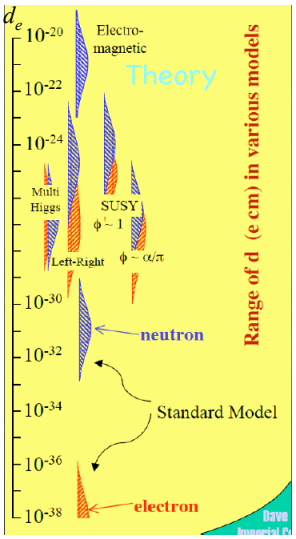

Principle of e-EDM measurement

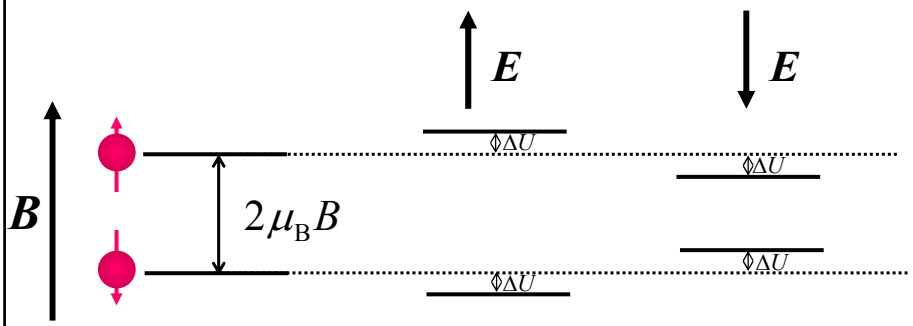

Interaction betweeen e-EDM (d_e) and the electric field $H = -\boldsymbol{d}_e \cdot \boldsymbol{E}$

Frequency shift due to the E field $\delta = \frac{4\Delta U}{\hbar} = \frac{4 d_e E}{\hbar}$

Search for e-EDM with atoms

$$\Delta U = -\boldsymbol{d}_{\text{atom}} \cdot \boldsymbol{E} = -R\boldsymbol{d}_e \cdot \boldsymbol{E}$$

R: enhancement factor $\propto Z^3$

114 for Cs (Z=55)

585 for Tl (Z=81)

1150 for Fr (Z=87)

Experiment using Tl atoms

$d_e < 1.6 \times 10^{-27}$ e cm

Commins, Ross, DeMille, Regan

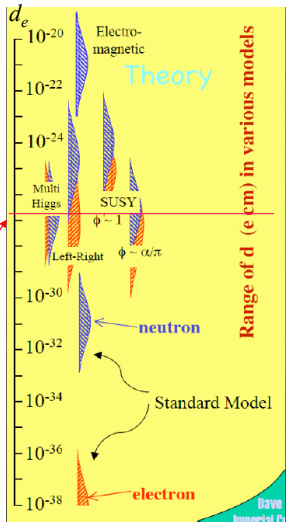

ラムゼー共鳴法

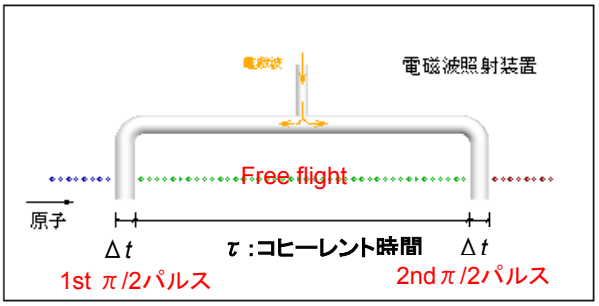

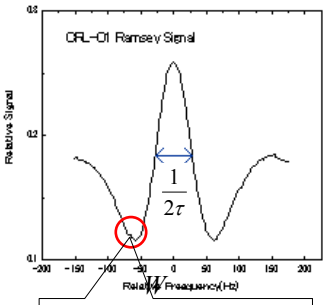

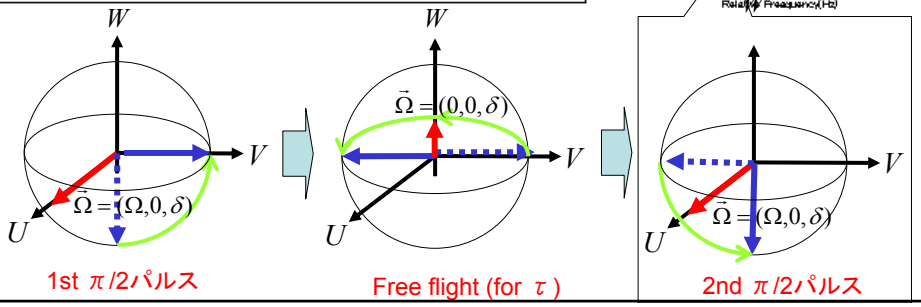

Cs fountain atom clock

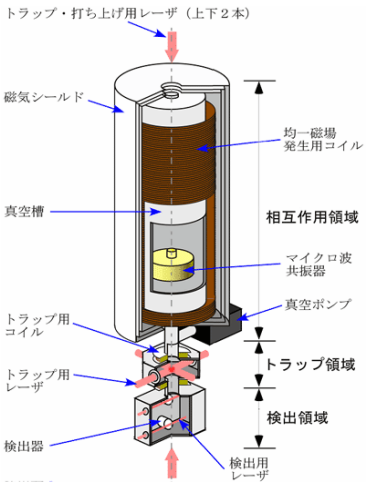

http://www.aist.go.jp/aist_j/press_release/pr2003/pr20030609/pr20030609.html

Ramsay fringe of atomic fountain

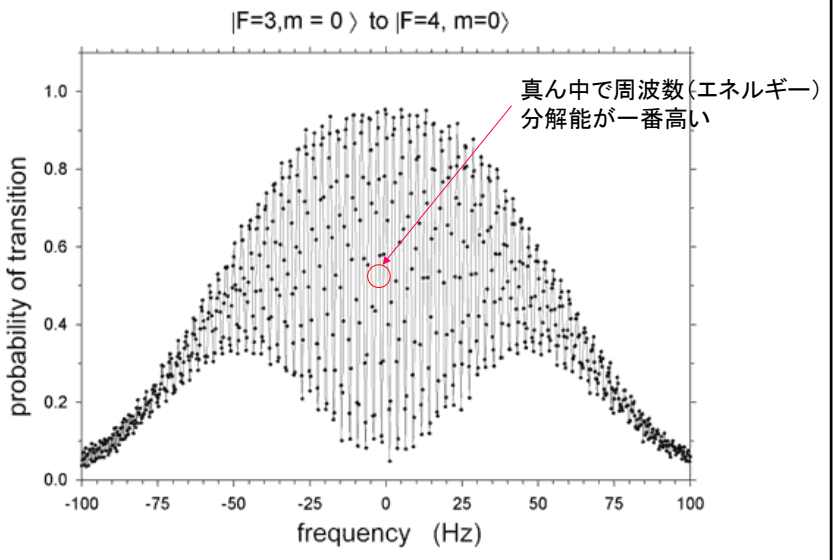

http://physics.nist.gov/TechAct.Archive/TechAct.98/Div847/div847h.html

Frequency uncertainty (projection noise) of Ramsay interferometer

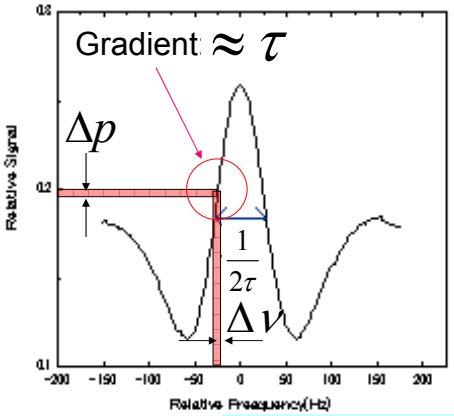

In case of using a trapped atoms (molecule)

N # of atoms in a trap

τ Time for a Single measurement

T Total (integrated) observation time

# of all measured atoms

Uncertainty of probability

$$\Delta p \approx 1/\sqrt{N \cdot \frac{T}{\tau}} \rightarrow \Delta\nu = \frac{\Delta p}{\tau} = \frac{1}{\sqrt{NT\tau}}$$

SERF(spin-exchange relaxation-free)

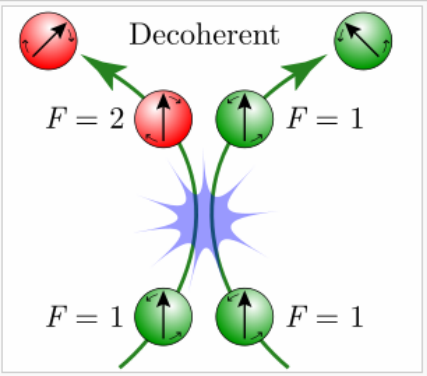

Alkali metal atoms with hyperfine state indicated by color precessing in the presence of a magnetic field experience a spin-exchange collision which preserves total angular momentum but changes the hyperfine state, causing the atoms to precess in opposite directions and decohere.

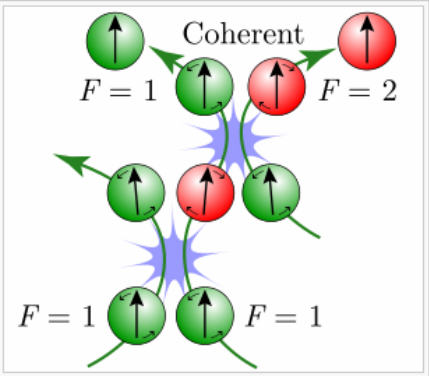

Alkali metal atoms in the spin-exchange relaxation-free (SERF) regime with hyperfine state indicated by color precessing in the presence of a magnetic field experience two spin-exchange collisions in rapid succession which preserves total angular momentum but changes the hyperfine state, causing the atoms to precess in opposite directions only slightly before a second spin-exchange collision returns the atoms to the original hyperfine state.

High-Sensitivity Atomic Magnetometer Unaffected by Spin-Exchange Relaxation

J. C. Allred and R. N. Lyman
Department of Physics, Univerisity of Washington, Seattle, Washington 98195

T. W. Kornack and M. V. Romalis*
Department of Physics, Princeton University, Princeton, New Jersey 08544
(Received 6 March 2002; published 9 September 2002)

Alkali-metal magnetometers compete with SQUID detectors as the most sensitive magnetic field sensors. Their sensitivity is limited by relaxation due to spin-exchange collisions. We demonstrate a K magnetometer in which spin-exchange relaxation is completely eliminated by operating at high K density and low magnetic field. Direct measurements of the signal-to-noise ratio give a magnetometer sensitivity of 10 fT $Hz^{-1/2}$, limited by magnetic noise produced by Johnson currents in the magnetic shields. We extend a previous theoretical analysis of spin exchange in low magnetic fields to arbitrary spin polarizations and estimate the shot-noise limit of the magnetometer to be 2×10^{-18} T $Hz^{-1/2}$.

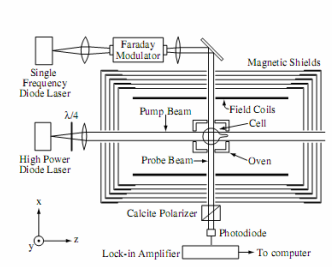

FIG. 1. Experimental implementation of the K magnetometer. Transverse polarization is detected using optical rotation.

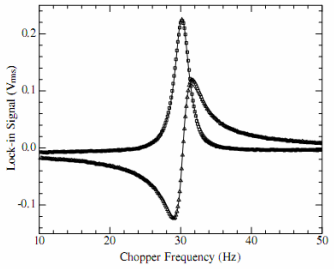

FIG. 2. Transverse resonance of the magnetometer. Both the inphase (squares) and out-of-phase (triangles) signals are shown. The fit is a Lorentzian with a half-width of 1.2 Hz.